# Unraveling the Piton de la Fournaise eastern flank structure by reconciling data from multiple geophysical methods

Quentin Dumont, Jean-Luc Froger, Marc Dumont, Lydie Gailler, Patrick Bachèlery, Valérie Cayol

Journal of Volcanology and Geothermal Research 473 (2026) 108579

Contents lists available at ScienceDirect

Journal of Volcanology and Geothermal Research

journal homepage: www.journals.elsevier.com/journal-of-volcanology-and-geothermal-research

# Unraveling the Piton de la Fournaise eastern flank structure by reconciling data from multiple geophysical methods

Quentin Dumont [a,b,*], Jean-Luc Froger [c], Marc Dumont [d], Lydie Gailler [b], Patrick Bachèlery [b], Valérie Cayol [b]

[a] Solid Earth Physics Laboratory, Department of Geophysics, Graduate School of Science, Tohoku University, Sendai 980-8578, Japan
[b] Université Clermont Auvergne, CNRS, IRD, OPGC, Laboratoire Magmas et Volcans, F-63000 Clermont-Ferrand, France
[c] Université Jean Monnet - Faculté des Sciences et Techniques, Laboratoire de géologie de Lyon : Terre, Planètes, Environnement - UMR CNRS 5276 LGL-TPE, 42023 Saint-Etienne, France
[d] Institute of Earth Sciences, University of Lausanne, Lausanne, Switzerland

ARTICLE INFO

*Keywords:*
Piton de la Fournaise
Flank instability
Ground deformation
Magnetic anomaly
Lineaments
Structural

ABSTRACT

The internal structure of volcanoes controls their volcano-tectonic evolution, especially during flank failure events. At Piton de la Fournaise volcano (La Réunion), offshore debris avalanche deposits, recent eastern flank slip events, and a seaward spoon-shaped preferential intrusion zone, demonstrate the recurrence of destabilization processes at different timescales. The stability of the eastern flank is therefore one of the major concerns at that volcano. To constrain the flank structures and destabilization mechanics, we compare the pattern of morphologic lineaments with recently published InSAR deformation measurement and modelling, magnetic anomalies, and seismicity data. We identify several structural discontinuities distributed in two families striking N50–80° and N120–160°. Their spatial location being limited to the eastern flank, we suspect the discontinuity as being the result of local intra-caldera processes or inheritance from caldera formation. Among these discontinuities, a major N65° discontinuity runs through the middle of the eastern flank, separating a north-western block from a south-eastern block. The north-western block shows low seismic velocities and is affected by sheared sill intrusions, while the south-eastern block shows higher seismic velocities and is affected by fault slip and creep. Both blocks probably lie between 0.5–2 km depth, at the base of a previously identified spoon-shaped intrusion zone around sea level. Both observed slip behaviours (sheared sill and faults) could be due (1) to an underlying intrusive complex creating a mechanical contrast and forming the N65° fault, or (2) to an edifice decoupling due to the N65° fault. Whatever the origin of the identified discontinuities, their presence and their interactions with the volcanic activity could lead to complex dismantling dynamics that should be accounted for in flank failure hazard assessment.

## 1. Introduction

Polygenic volcanoes result from a succession of constructive and destructive phases occurring over hundreds of thousands of years. This alternation induces a complex internal structure associated with a surface morphology that may reflect underlying discontinuities. The internal structure of volcanic edifices is one of the major factors controlling eruptive activity, morphological evolution, and associated hazards (Solaro et al., 2010; Boudoire et al., 2017; Walter et al., 2019). Structural discontinuities can contribute to the channelling and orientation of magmatic intrusions (Delaney et al., 1986; Valentine and Krogh, 2006; Martínez-Poza et al., 2014; Ruch et al., 2016; Drymoni et al., 2021), in association with the stress field (Nakamura, 1977; Rubin and Pollard, 1988; Rivalta et al., 2015). They could also control hydrothermal fluid migration or gas migration (Barde-Cabusson et al., 2012; Boudoire et al., 2017). During partial destabilizations, discontinuities can be activated as earthquakes, slow slip events, or stable slip. These relative displacements often occur at major interfaces below the edifice (interface with the oceanic crust as in Hawaii; Denlinger and Morgan, 2014; or with a sedimentary substratum as at Mount Etna; Tibaldi and Groppelli, 2002; Palano, 2016), or within the edifice along pre-existing discontinuities such as fractures, faults, or ductile horizons (i.e., hydrothermally altered rocks, hyaloclastite or pyroclastite layers; Siebert, 1984), or along sill injections path such as at the Piton des Neiges volcano (Famin et al., 2016; Chaput et al., 2017).

At Piton de la Fournaise volcano (La Réunion), one of the major hazards is the occurrence of flank collapse. Evidence of recurrent large

* Corresponding author at: Solid Earth Physics Laboratory, Department of Geophysics, Graduate School of Science, Tohoku University, Sendai 980-8578, Japan.
*E-mail address:* dumont.quentin.lucien.a1@tohoku.ac.jp (Q. Dumont).

https://doi.org/10.1016/j.jvolgeores.2026.108579
Received 23 October 2024; Received in revised form 17 February 2026; Accepted 23 February 2026
Available online 23 February 2026

collapses in the history of the volcano is indicated by (1) bathymetric studies showing the presence of debris avalanche and slump deposits with volumes up to 100 $km^3$ (Oehler et al., 2004, 2008); and (2) presence of large seaward horseshoe-shaped collapse scars in the morphology of the edifice, interpreted as remnant of lateral collapse by some authors (Duffield et al., 1982; Labazuy, 1996; Oehler et al., 2008). Instability of the eastern flank was proposed since the 1980s, mainly on the basis of geomorphological interpretations (Bachèlery, 1981; Duffield et al., 1982; Michon et al., 2016). More recently, Interferometric synthetic Aperture Radar (InSAR) data has allowed detection of large eastward (i.e. seaward) displacement in the eastern flank related to five co-intrusive slip events (Dumont et al., 2022, 2024). The displacement in each event can reach a meter (Froger et al., 2015; Dumont et al., 2022). Moreover, these slip events have been interpreted to occur along a seaward spoon-shape intrusion zone (Dumont et al., 2022), where dike intrusions at the head of the structure favours the occurrence of slip (Dumont et al., 2024). This structure has been interpreted as a potential destabilization surface where accumulation of meter-scale intrusion and coeval slip can lead to catastrophic flank collapse. Such a collapse could induce tsunami, which could significantly affect La Réunion and the neighbouring Mauritius Island (Kelfoun et al., 2010). However, although the main instability zone is located on the eastern flank, the internal structure of the flank and the presence of potential discontinuities as suggested by its morphology, remains poorly understood.

The purpose of this study is to better characterize the structure of the eastern flank, its relation with the spoon-shaped intrusion zone, and thus to better identify the mechanisms and features that control the stability of the flank and its potential for collapse. We conduct a structural study relying on currently published morphological lineaments and geophysical observations of the volcano's eastern flank, including analysis of eruptive fissure locations, InSAR displacement measurements and modelling, magnetic anomalies, and seismicity. Joint analysis of the data reveals contrasting mechanical behaviours between a north-western block dominated by intrusive processes and an unstable south-eastern block affected by long-term steady slip and sudden slip.

## 2. Geological context

### 2.1. Piton de la Fournaise volcano

Piton de la Fournaise volcano forms the south-eastern side of La Réunion Island (Indian Ocean). La Réunion Island results from the activity of the hotspot responsible for the Deccan Traps (Duncan et al., 1989). The north-west flank of Piton de la Fournaise volcano is buttressed by the older volcanic edifice of Piton des Neiges (Fig. 1a). To the east, the volcano is assumed to be underlain by an intrusive mafic complex, considered as the remnant of an older edifice called Proto-Fournaise or Les Alizés volcano (Lénat et al., 2012a), which was inferred on the basis of geological data provided by a borehole (Rançon et al., 1989) and by gravity studies (Rousset et al., 1989; Malengreau et al., 1999; Gailler et al., 2009).

The history of Piton de la Fournaise has been punctuated by at least five large destructive collapse events whose scars delimit horseshoe-shaped depressions open towards the east (Bachèlery and Mairine, 1990; Oehler et al., 2008; Merle et al., 2010). The most recent collapse created the Enclos Fouqué - Grandes Pentes - Grand Brûlé complex (<4500 yr BP, Bachèlery, 1981; Mohamed-Abchir, 1996; Ort et al., 2016; see Fig. 1a) with dimensions of 8 km (N-S) by 13 km (W-E), delimited by steep walls of 100 to 200 m high. However, the mechanism behind these collapse events is still debated. As proposed for the youngest event, they could be related to either vertical collapse (related to some magma reservoir emptying) or a lateral flank collapse, or a combination of both (Michon et al., 2016).

Located inside the Enclos Fouqué caldera, the current volcanic center has formed a 400 m high central cone with a 1 km wide and 300 m deep summit crater (the Dolomieu crater; Fig. 1a). To the west, the volcano shows gently sloping terrains, while the eastern flank is characterized by steep slopes, locally reaching 35° towards the ocean. This area, called the Grandes Pentes, is interpreted as resulting from either the juxtaposition of several seaward slip fronts (Bachèlery, 1981), from tilted blocks sliding on the roof of the intrusive complex of Les Alizés (Merle and Lénat, 2003), or from the hydrothermal system subsidence and lateral spreading under the effect of the weight of the edifice (Michon and Saint-Ange, 2008). In the northern side of the Grandes Pentes, the Plaine des Osmondes and the Piton de Crac are other prominent structures (Fig. 1). The Plaine des Osmondes is a depression possibly originating from a recent collapse and/or associated with headward erosion from a paleo-river (Bachèlery, 1981; Courteaud, 1996; Michon and Saint-Ange, 2008). The Piton de Crac separates the Plaine des Osmondes to the north from the Grandes Pentes to the south. It is a peak of lava older than the Enclos Fouqué formation (13 ± 6 kyr at its base, Gillot et al., 1994), which could be either an autochthonous remnant of the ancient Piton de la Fournaise edifice (Bachèlery, 1981; Michon and Saint-Ange, 2008) or an allochthonous block transported by a lateral collapse (Labazuy, 1996; Oehler et al., 2004).

After six years of rest, volcanic activity resumed at Piton de la Fournaise in 1998 (Peltier et al., 2009; Roult et al., 2012). Between 1998 and 2023, 63 intrusions have emplaced in the shallow edifice, inducing seismic crises and significant surface displacements, 59 of which resulted in an eruption. Eruptions generally take place along eruptive fissures that open along one of the rift zones radiating around the central cone (Villeneuve and Bachelery, 2006). The main rift zone (Fig. 1a) of the edifice has a general arcuate NE-SE orientation passing through the Dolomieu crater (Bachèlery, 1981; Michon et al., 2007, 2009, 2015; Peltier et al., 2015b). This rift zone extends outside the walls of the Enclos Fouqué caldera, but in a much more diffuse and less active way (Bachèlery, 1981; Stieltjes and Moutou, 1989; Lénat et al., 2012a). In addition to this main rift zone, secondary rift zones with N60° and N120° orientations start at the south-eastern boundary of the Dolomieu crater (Michon et al., 2015). Some secondary intrusive axes trending N210° and N300° were also evidenced to the SW and NW of the summit cone from eruptive fissure and cone density (Bonali et al., 2011; Michon et al., 2015) and InSAR displacement inversions (Dumont et al., 2022), but are less well constrained due to their lower activity.

In March–May 2007, the largest eruption of the last hundred years took place on the lower eastern flank of the volcano. InSAR showed that the eruption was associated with an eastward slip of the eastern flank of the volcano of up to 1.4 m (Froger et al., 2015). Post-eruptive displacements successive to this event was characterized by an eastward subsidence following an exponential decrease during about 1–3 years (Froger et al., 2015; Chen et al., 2017). Starting from 2011, the eastern flank slip have reached a steady state at a continuous slip rate of 1.5 cm/yr (Peltier et al., 2015a; Chen et al., 2017; Poland et al., 2017), which accelerates with magmatic activity. We will refer to as the steady state long-term slip.

### 2.2. Previously identified structures in the eastern flank

#### 2.2.1. Morpho-structural analysis

The main lineaments of the eastern flank were determined by Michon and Saint-Ange (2008) from morphological analysis of the topography, based on local changes in slope steepness and orientation. Proposed lineaments are reported in Figs. 1 and 2 on slopes and aspect maps. The two main lineaments, oriented N65° and located south of the summit cone (lineaments 1 and 2 in Figs. 1 and 2), are associated to a local change in slope resulting in a ≈100 m vertical offset between the north-west and the south-east (Fig. 2e). Michon and Saint-Ange (2008) interpreted these structures as surface deformation due to normal faults. They are connected to a V-shaped topographic feature formed by two smaller lineaments materialized by two areas of steep slopes 2 km south of the Piton de Crac (lineaments 3 and 4). Two

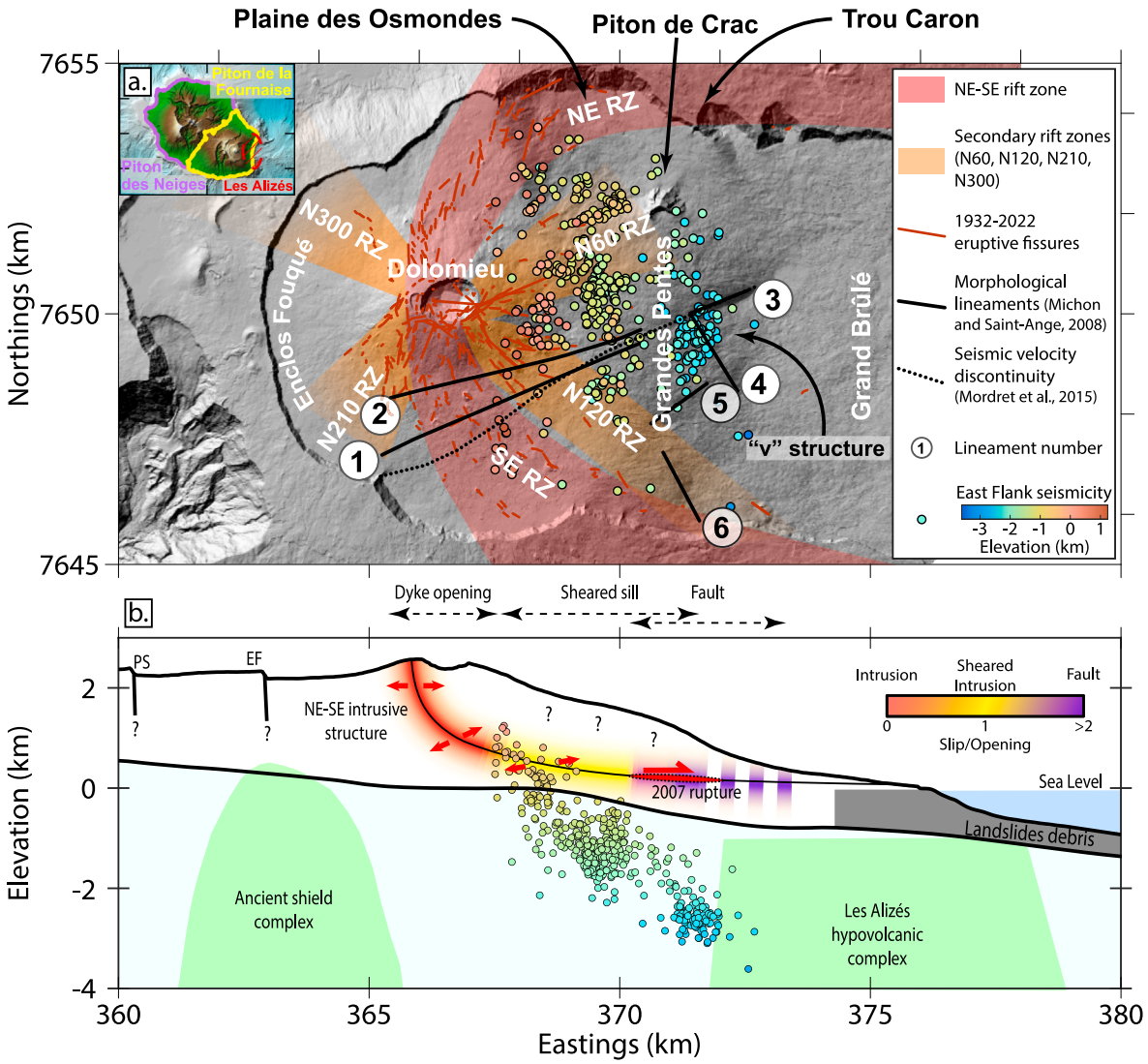


**Fig. 1.** **a.** Piton de la Fournaise shaded topography and locations discussed in the text. The inset in the top left corner shows the location of the volcanic edifices on Réunion Island. **b.** Cross-section interpretative view of the internal structure. Modified from Lénat et al. (2012a) and Dumont et al. (2022). Expected base of the edifice (around sea level) comes from Gailler and Lénat (2012).

similar lineaments, south of the previous ones, form a slightly more open and less marked V-shape in the topography (lineaments 5 and 6). These morphological lineaments are interpreted as evidence of normal faults that could (1) accommodate the subsidence of the intrusive complex of Les Alizés (Michon and Saint-Ange, 2008) or (2) represent the headwall of landslide units of the Grand Brûlé slip zone (Bachèlery, 1981; Merle and Lénat, 2003).

### 2.2.2. *Internal structural features deduced from geophysical data*

The internal structure of Piton de la Fournaise has been the subject of several studies especially through geophysical investigations using seismic, electrical resistivity, electromagnetic, gravimetric and displacement data (Lénat et al., 2012a). However, most of them were mainly focused on the area beneath the central cone (Gailler et al., 2009) or the western plains (Plaine des Sables; Gailler et al., 2018), due to the difficult access on the Grandes Pentes and the Grand Brûlé. These studies provided information on the plumbing system, interpreted as a sub-vertical conduit located 500–1000 m west of the summit between −5 km and sea level (Battaglia et al., 2005; Prôno et al., 2009; Lengliné et al., 2016; Beauducel et al., 2020) and by a shallow storage zone postulated to be around sea level (Battaglia et al., 2005; Peltier et al., 2016; Beauducel et al., 2020). At shallower level, other studies have helped to constrain the structure of the summit cone and the hydrothermal system below the Dolomieu crater (Lénat et al., 2000; Barde-Cabusson et al., 2012; Lénat et al., 2012b; Dumont et al., 2019).

In the eastern flank of Piton de la Fournaise, information on the deep structure is much scarcer than in the summit area and is derived from seismic data, magnetic surveys and deformation studies. Small volcano-tectonic earthquakes are reported beneath the eastern flank (average duration magnitude of $M_d$ = 0.8 ± 0.5), especially during eruptions (Lénat et al., 1989, 2012a; Duputel et al., 2021). Their location defines a surface dipping ≈45° to the east (Fig. 1b), with a slight curvature in the north-south direction. This location contrasts with the common pre-eruptive seismic crisis typically forming a cluster beneath the summit crater (Duputel et al., 2021). The origin of the eastern flank seismicity is still poorly understood, and no focal mechanisms have been determined, but it is suspected to be triggered by magma chamber inflation (Gerbault et al., 2022) or dyke intrusions (Dumont et al., 2024). In addition to earthquake locations, the S-wave velocity anomalies inverted by Mordret et al. (2015) show that, in the first 100 m depth below the surface, the summit cone and the north-west flank are characterized by low seismic velocities, while the south-east flank shows higher velocities. Mordret et al. (2015) noticed that

these two regions are delimited by a rapid change in velocity, following a ≈N60° orientation, in a zone corresponding to the N65° fault identified by Michon and Saint-Ange (2008) (lineament 1 in Fig. 1). However, this velocity change does not extend to greater depth. In addition, Martelet et al. (2014) conducted an airborne time domain electromagnetic survey from which (Dumont et al., 2019) computed an electrical resistivity model of the volcano down to 1 km depth. From 400 m to 1 km depth, they showed that vertical sharp contrasts in resistivity are present beneath lineaments 3 and 8 (Fig. 2), which may be indicative of discontinuities. For lineaments 1 and 2, the presence of rift zones nearby complicates the interpretation of the resistivity model. However, a vertical conductive discontinuity is imaged beneath lineament 2 from the surface to a depth of 1 km.

Finally, the recent 3D inverse modelling of the InSAR displacement of 57 intrusions that occurred between 1998 and 2020 shed a new light on intrusive activity in the eastern flank and on its stability (Dumont et al., 2022). Most intrusions were found to be emplaced in a preferential spoon-shaped zone such that vertical dikes intrude in the NE-SE rift zone and that horizontal sills intrude beneath the eastern flank between 0 and 1 km above sea level (Fig. 1). This structure is undergoing pure opening at the head of the structure, slip coeval with opening further east, and slip only in its easternmost and lowermost part. Since 1998, five slip events have been observed in the eastern flank (Dumont et al., 2022, 2024). The occurrence of slip indicates that the sills are not perpendicular to the least principal stress, probably because they are guided by a pre-existing discontinuity similarly to field observations on the nearby extinct volcano, Piton des Neiges (Famin and Michon, 2010; Berthod et al., 2016). Considering uncertainties, Dumont et al. (2022) proposed that this discontinuity could correspond to the expected base of the Piton de la Fournaise edifice (around sea level), as determined by Gailler and Lénat (2012) from aeromagnetic and gravimetric surveys.

## 3. Data

Structural elements identified previously, principally through morpho-structural analysis, only give information of the surface structures and do not necessarily reflect deeper structures of the eastern flank (Torgersen et al., 2024). To improve our knowledge of the internal structure of the eastern part of the volcano, we have analysed a set of recently published geophysical data including InSAR displacement data and derived models, magnetic data and seismicity, together with previous morpho-structural data and eruptive fissure locations. While these data were previously interpreted independently and with no particular focus to the eastern flank, we here re-examine them jointly to propose an integrated conceptual model of the eastern flank. We relate surface characteristics, from morpho-structural lineaments, to a deeper geological significance by assuming that geophysical signal showing strong gradients that extend on a sufficient distance along a given direction could be considered as indicative of structural discontinuities extending to greater depth (i.e. between the surface to depths ≥1 km).

### 3.1. Morphological lineaments

Based on a careful re-examination of a recent 5 m LiDAR digital elevation model produced in 2008 by the French National Geographic Institute, we have confirmed the lineaments already described by Michon and Saint-Ange (2008), and have integrated other remarkable features (Fig. 2). Starting from the north of the Enclos Fouqué, two lineaments, oriented N160° and N70°, correspond to the east-north-east and south-south-east escarpments of the Plaine des Osmondes (lineaments 7 and 8; Fig. 2). They are marked by steep slopes of up to 30–40°. Their orientation and slope values are similar to those of the lineaments identified by Michon and Saint-Ange (2008) in the Grandes Pentes area. Similarly, at the eastern end of the Plaine des Osmondes, another area with slopes greater than 20° is oriented in the N160° direction (lineament 9; Fig. 2). In the south-east continuation of this lineament, the slopes decrease to 15°–20° but still have a N160° orientation. This N160° lineaments is almost parallel to the lineament 7, further uphill. Along the eastern edge of the Piton de Crac and further south-east, a strong slope discontinuity shows a very clear linear extension oriented N130° (lineament 10; Fig. 2). Furthermore, this lineament is associated with a change in the orientation of the lines of greatest slope, from N60–80° to the south-west of the lineament to N100–120° to the north-east. The change in slope orientation extends north-west of the Piton de Crac, potentially indicating a continuation of the lineament further north-west (Fig. 2b). Finally, a last lineament trending N120° can be identified at the south-western limit of the summit cone (lineament 11; Fig. 2). It is characterized by both a rapid change in slope (from slopes higher than 20° to less than 10°) and a change in slope orientation (from ≈N180° to N120–160°). Since the characteristics of the new lineaments described above are consistent to those of Michon and Saint-Ange (2008) in terms of orientations and slope values, we considered them of interest and added them to the set of lineaments to be compared with the geophysical data. It leads to a total of 11 lineaments to be analysed.

### 3.2. Deformation data and modelling

Through their modelling, displacements data provide information on the nature (massive reservoir or dislocation), the location and the mechanism (opening or shear) of the displacement source(s). They are also sensitive to differential movements allowing the detection of active buried faults or discontinuities and the mapping of structural block (Solaro et al., 2010; Bonforte et al., 2011; Froger et al., 2015; Tridon et al., 2016; Camacho et al., 2020). Moreover, displacements allow the localization of intrusions, which can indicate weakness zones in the edifices, especially in the case of preferentially oriented intrusions such as at Piton de la Fournaise.

Since 2003, the Indian Ocean InSAR Observatory ($OI^2$), a component of the French National Observation Service ISDeform (INSU/CNRS), carries out a continuous InSAR monitoring of the displacement of Piton de la Fournaise volcano (Richter and Froger, 2020). Thanks to this service, all magma injections in the shallow edifice have been imaged by at least one interferogram since 2003. Moreover, the 23 year long temporal coverage of the radar image acquisitions allowed both the exhaustive characterization of the 57 magma intrusions through inverse modelling of co-eruptive displacements (Fukushima et al., 2005, 2010; Tridon et al., 2016; Smittarello et al., 2019; Q. Dumont et al., 2021; Dumont et al., 2022) and the long-term monitoring of the eastern flank deformation through time series computations (Chen et al., 2017). In order to obtain relevant information on the internal structure of the eastern flank, we focus (1) on co-eruptive displacements related to slip events in the eastern flank as well as their inverse modelling performed by Dumont et al. (2022, 2024), and (2) on structural analysis of long-term slip computed by Chen et al. (2017).

### 3.3. Magnetic data

Since magnetization is sensitive, among other parameters, to alteration associated with fluids and fracturing, magnetic measurements are powerful in imaging mechanical heterogeneities (Gailler and Lénat, 2012; Gailler and Kauahikaua, 2017; Bouligand et al., 2019). Magnetic mapping has been shown to be particularly useful for the detection and delineation of volcanic structures (M. Dumont et al., 2021).

Here, we use the map of magnetic anomalies reduced to the pole (RTP map) made by Martelet et al. (2014) and Dumont et al. (2019) from the ReunEM airborne electromagnetic survey campaign carried out in 2014 by the French Geological Survey (BRGM). The raw magnetic data were processed to remove (1) the regional gradient of the earth's magnetic field using the International Geomagnetic Reference Field model (IGRF), and (2) the signal bias from flight orientation

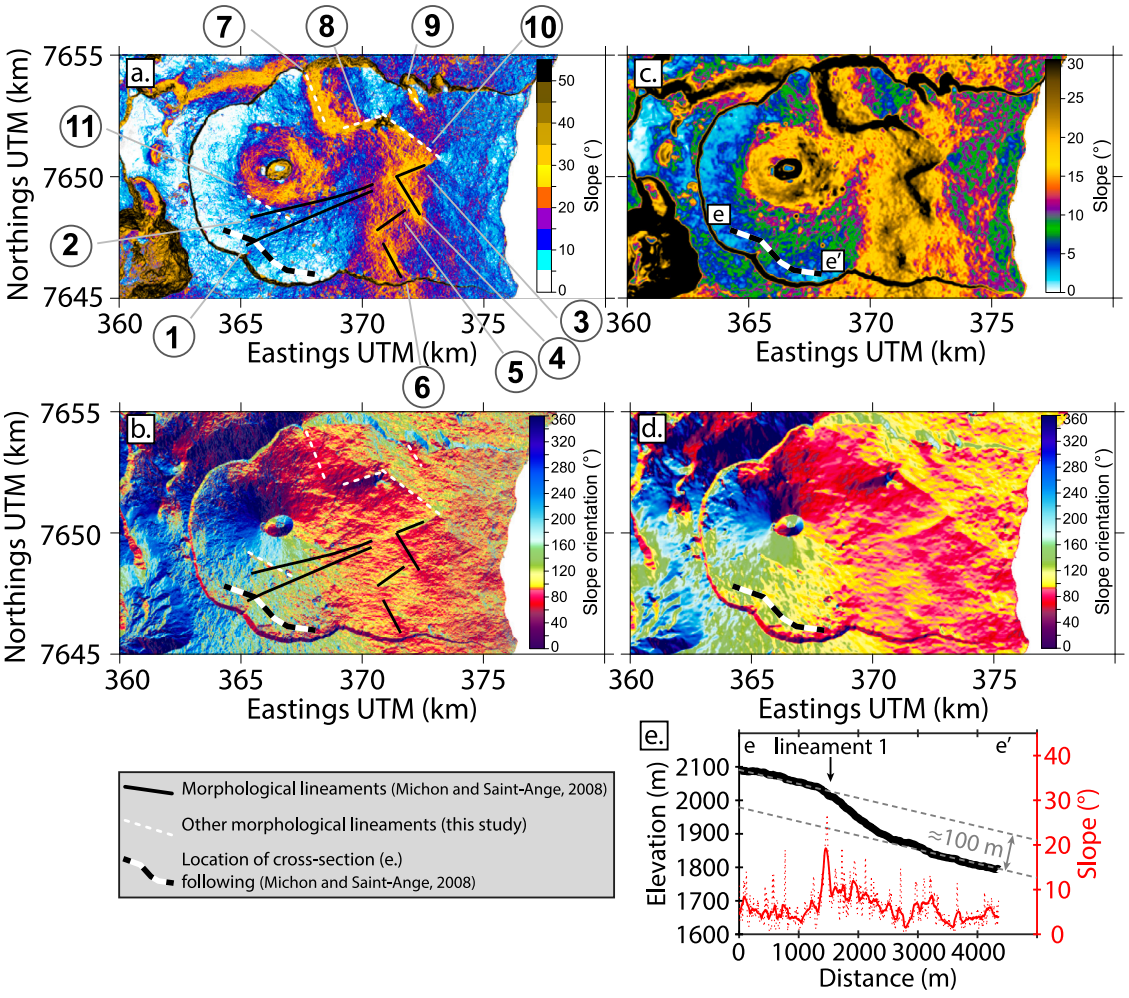


**Fig. 2.** Morphological features of Piton de la Fournaise. (**a.**) and (**b.**) give slope and slope orientation maps together with identified lineaments (numbered as discussed in the text). (**c.**) and (**d.**) provide the same maps as (**a.**) and (**b.**) but smoothed using a 50 m moving window averaging. (**e.**) Cross-section intersecting lineament 1 illustrating slope change and vertical offset (Michon and Saint-Ange, 2008). Red curves give slopes (dashed) and 50 m moving window averaged slopes (plain). Elevation data come from a 5 m LiDAR digital elevation model produced in 2008 by the French National Geographic Institute.

and diurnal variations thanks to ground magnetic monitoring at a permanent station in a low magnetic disturbance area during the survey (Martelet et al., 2014). After this first processing, the reduction to the pole recalculates the anomalies with a vertical magnetic field to delete magnetic anomaly bipolarity and vertically align anomalies above their sources on the final RTP magnetic anomaly map (Baranov, 1957).

In addition, we used local phase filters of the RTP map to enhance the horizontal and vertical locations of the magnetic anomaly sources. To better identify local magnetized structures, we relied on the vertical derivative of the RTP map (Elkins, 1951). The vertical derivation enhances the shorter wavelengths of the spatial variations of the magnetic signal as well as the noise. Thus, the vertical derivative focuses on the surface formations highlighting shallow sources and local demagnetization potentially indicative of faults (Fitterman, 1979; Adler et al., 1999).

### 3.4. Seismicity

We also use seismicity data as they provide information on stress perturbation, fluid migration or pre-existing fracture plane locations and orientations. We rely on earthquake hypocenter located by the Observatoire Volcanologique du Piton de la Fournaise (OVPF/IPGP). We focused on the seismicity of the eastern flank, which can be easily isolated from the seismicity located beneath the summit crater (Duputel et al., 2021). Events locations shown in this study span between May 2012 and December 2021. They are restricted to only the area within the Enclos Fouqué (Duputel et al., 2021), where the lineaments are observed.

### 3.5. Eruptive fissure locations

The location and orientation of eruptive fissures can provide insights into the orientation of principal stress axes or the presence of weakness zones within the volcanic edifice. To investigate any relations between eruptive activity and potential identified structures, we use eruptive fissure locations since 1931 provided by OVPF, and compute an eruptive fissure density map using a circular kernel of 500 m of diameter (Fig. 3i).

## 4. Data analysis

In the following, we describe the major features observed in each of the data set considered.

### 4.1. Co-eruptive slip

Since 1998, five slip events have been detected through inverse modelling of InSAR data (Dumont et al., 2022). All of them took place beneath the eastern flank of the volcano, in the Grandes Pentes area or in the Plaine des Osmondes area. They all show eastward surface displacements going up to 0.5–1.4 m. All are associated with 0.25–0.6 m of uplift or show both uplift and subsidence (displacements for each event are given in Supplementary Material). Two distinct destabilization mechanisms were determined by inverse modelling: (1) slip induced by sheared sills (i.e. sub-horizontal magmatic sheet intrusion affected by co-intrusive shear deformation) and (2) slip on a sub-horizontal fault in the continuity of the NE-SE spoon-shaped intrusive structure beneath the eastern flank. The January 2004, September 2020, and October 2021 intrusions were characterized by a shear stress drop of the same order of magnitude as their overpressure (Fig. 3a,b, and Supplementary Material). For these events, the modelled intrusions indicate fracture opening and slip of 1.5–1.8 m (Dumont et al., 2022). Such characteristics are typical of sheared sills (Chaput et al., 2014). In contrast, the modelling of March–April 2007 and October 2019 events indicates almost exclusively shear stress drop (Fig. 3a,b and Supplementary Material). For the March–April 2007, the overpressure is negligible (Cayol et al., 2017). The slip and opening on the modelled plane reaches 2 m and 0.4 m, respectively. The October 2019 event consists of two parts: a sill part under the summit is subjected solely to overpressure; whereas, a fault part, to the east, is affected by a shear stress drop 16 times higher than the overpressure leading to a slip of about 1 m towards the east for 0.1–0.2 m of opening. Slip events in March–April 2007 and October 2019 thus both show a fault behaviour.

Despite the coexistence of both slip mechanisms, we observe that they affect different regions of the edifice. The sheared intrusions (January 2004, September 2020, and October 2021) affect the northern part of the Grandes Pentes and the Plaine des Osmondes while the faults are located in the central and southern sectors of the Grandes Pentes.

The cumulated eastward displacement map (Fig. 3c) of the five slip events shows eastward displacements characterized by a uniform displacement field on the entire eastern flank of the volcano, with a maximum of displacement located in the central part of the Grandes Pentes, 500 m to the west of the V-shaped structure. On the other hand, the vertical displacement map (Fig. 3d) shows a more complex displacement field. A region of large inflation is localized only in the northern half of the edifice, starting from the Dolomieu crater and extending north-eastward to the Plaine des Osmondes and the Piton de Crac. South of the large inflation area, a region affected by very low inflation, or even subsidence, is extending up to the southern walls of the caldera. The transition between these two regions occurs along a roughly N60° trending axis which corresponds to the transition between both slip mechanisms.

### 4.2. Steady state long-term slip

Following the exponential decrease of the March–April 2007 post-eruptive displacements, slip continued in a steady state at a rate of 1.5 cm/yr (Peltier et al., 2015b; Chen et al., 2017). In the east–west and vertical displacements maps derived from InSAR by Chen et al. (2017) (Fig. 3e,f), we observe a widespread sector ($\approx$ 20 km$^2$) affected by downward and eastward motion in the Grandes Pentes. These displacements are stronger in the southern half of the Grandes Pentes, where a fault slip mechanism is highlighted by co-eruptive displacements modelling (Fig. 3a,b). To the south, displacements suddenly stop along a N120° trend. In contrast to the Grandes Pentes, the summit area and the Plaine des Osmondes area show mainly subsidence interpreted by Chen et al. (2017) and Hrysiewicz (2019) as due to summit deflation and thermo-mechanical contraction of lava flows.

### 4.3. Magnetic anomaly

The main feature of the RTP magnetic anomaly map is a high magnetic anomaly (> 2000 nT) corresponding to the summit area and extending eastward, splitting into two branches to the north-west and south-west of the V-shaped structure (Fig. 3g). The boundary between the northern and southern branches of high magnetic anomaly is marked by a strong decrease of the magnetization especially to the east, where magnetization values decrease from 3000 nT (to the west) to −1000 nT (to the east). The eastern continuation of the summit positive anomaly ends by a sudden drop of the magnetization at the base of the Grandes Pentes leading to negative anomalies in the coastal part of the Grand Brûlé. In the southern part, the limit of the strong positive magnetic anomaly is elongated along a N110–120° trend. The steep slopes towards the Plaines des Osmondes are characterized by strong gradients in the magnetic anomaly map along the escarpments (Fig. 3h). In the vicinity of the caldera walls, strong negative anomalies are observed, contrasting with the central part of the Enclos Fouqué, showing high magnetization.

### 4.4. East Flank seismicity

As described previously, the seismicity occurring in the eastern flank aligns along a 45° eastward dipping plane, where the locally higher seismic activity forms clusters (Fig. 1b). On a map view (Figs. 1a and 3i), seismicity shows a significant concentration of earthquakes forming clusters in the middle of the Grandes Pentes. Especially, close to the V-shaped structure, we observe a large seismic cluster. Another cluster, elongated in the SW-NE direction, is found along the south-east escarpment of the Plaine des Osmondes. To the north and west of the Plaine des Osmondes, the seismicity becomes much scarcer. Comprised between the Plaine des Osmondes and the lineament 1, another particularly important cluster is present under the Grandes Pentes. Few seismic events are observed to the south, close to the southern wall of the caldera. However, no significant seismicity is detected east of the Grandes Pentes.

### 4.5. Eruptive fissure density

At the summit scale, the fissure density map shows a very high density of eruptive fissures (>4 × 10$^{-3}$/m$^2$; Fig. 3i) in the summit part especially at the southern edge of the crater and on the east and south flank of the summit cone. It results from the local superposition of the summit portion of the SE, N120°, N60°, and N210° rift zones, together with some concentric fissures following the crater rim. The north-eastward continuation of this high-density area beyond the crater exhibits a sharp N60–70°-trending boundary, primarily controlled by the narrow N60° rift zone located to the north-east of the Dolomieu crater.

At a larger scale, the high fissure density (>1 × 10$^{-3}$/m$^2$, white contour on Fig. 3i) extends to the north along a narrow path clearly highlighting the NE rift zone up to the northern escarpment of the Plaine des Osmondes. However, we observe a contrasted behaviour for intrusion propagating to the south as the high fissure density area suddenly decreases south of the summit cone. Only a few fissures are found more to the south, and these few fissures align along a N120° trend.

## 5. Discussion

### 5.1. Compilation of the geophysical signals associated with the lineaments

The location of the morphological lineaments coincides with remarkable features in the deformation, the magnetic field, the seismicity, and the eruptive fissure locations. This coincidence suggests that the lineaments are representatives of geological structures extending

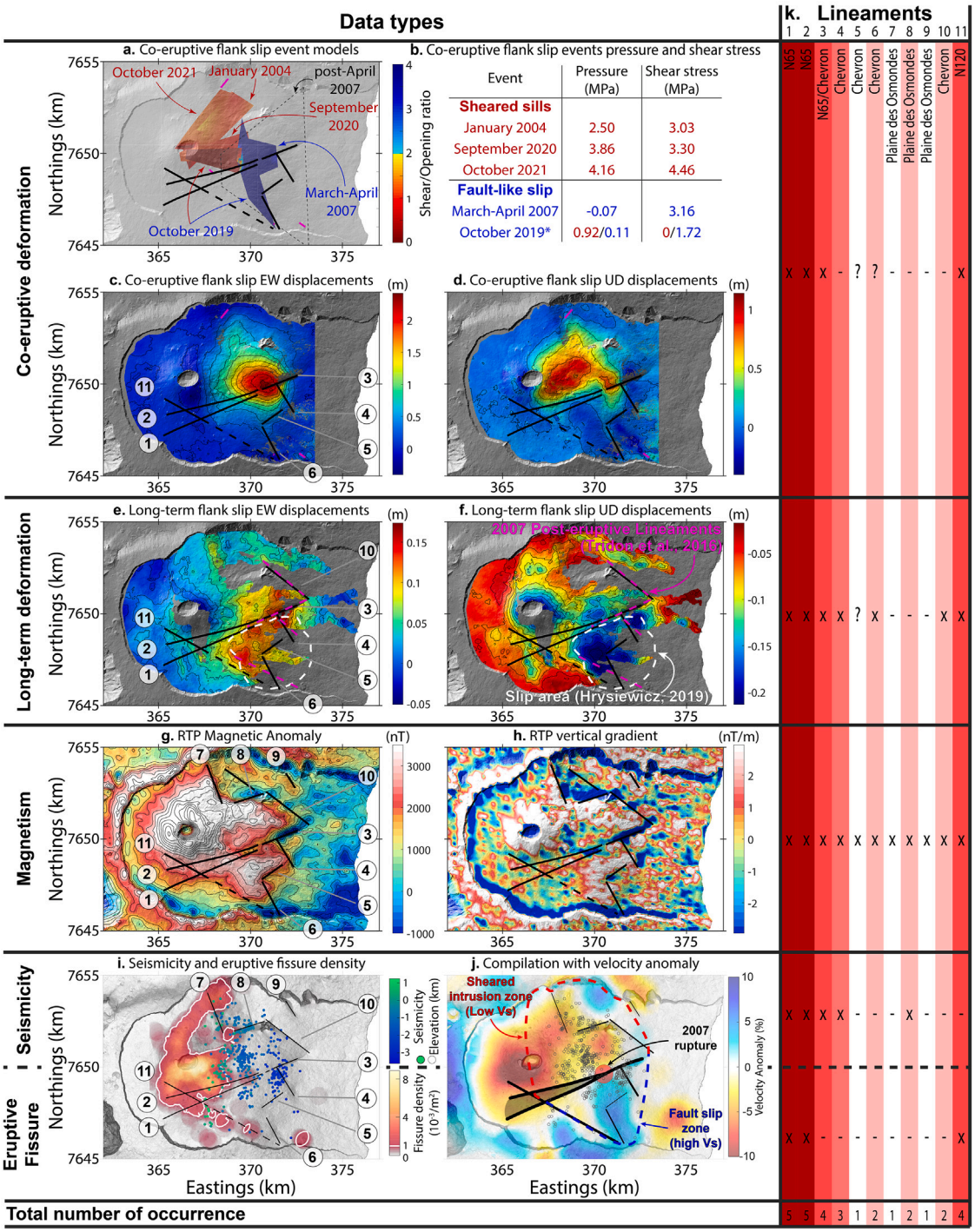


**Fig. 3.** Comparison between geophysical data and location of the morphological lineaments. **a.** Slip event models from Tridon et al. (2016), Cayol et al. (2017), Dumont et al. (2022, 2024) and relative pressure and shear stress associated with each models. Note that October 2019 model is composed of two sources with different characteristics. **c.** and **d.** Eastward (EW) and upward (UD) cumulated displacements related to the five slip events. **e.** and **f.** EW and UD long-term eastern flank displacement components between March 2009 and October 2014 (Chen et al., 2017). Note that lineaments from Tridon et al. (2016), in magenta, were previously identified on the March–April 2007 post-eruptive displacements not shown here. **g.** and **h.** Magnetic anomaly map reduced to the pole (RTP) and the related first vertical derivative. **i.** Seismicity of the eastern flank recorded between May 2012 and December 2021, together with the eruptive fissure density (white lines indicate density contour of $1 \times 10^{-3}/m^2$). **j.** S-wave seismic velocity anomaly (Mordret et al., 2015) together with the interpretative compilation of all lineaments. Their relative importance is represented by the thickness of the segment. It is assessed from the number of occurrence of the lineament for each data type as given on the side table **h.**. For all data types, black lines indicate the morphological lineaments, numbered as discussed in the text and as given in Fig. 2.

at greater depth of at least a few hundred meters. We summarize below the relation between each structure and the geophysical data (see detailed description for each data type in Supplementary Material). The number of occurrence of these structures in the different data sets was used to rank the structures by their relative importance (Fig. 3k).

#### 5.1.1. The N65° structure

We note that the structure appearing in all datasets is coincident with the three N65° lineaments in the central part of the Grandes Pentes (lineaments 1, 2 and 3, Fig. 3), which are hereafter considered together as the N65° structure. It corresponds to the fault described by Michon and Saint-Ange (2008). In addition to a topographic offset noted by these authors, the N65° structure also represents a boundary in the style of deformation at different time scales. It delineates the boundary between two distinct co-intrusive slip mechanisms with sheared sills to the north and fault slip to the south as shown: (1) by the InSAR-derived models (Fig. 3a–b) and (2) by the cumulated co-eruptive displacements where inflation is limited to the north-west of the N65° structure, whereas no inflation or a slight subsidence is observed to the south-east (Fig. 3c–d). During the March–April 2007 post-eruptive displacements, the N65° structure coincides with a strong gradient axis (Fig. 3e–f; Tridon et al., 2016). On longer time scale, it marks the northern limit of the area affected by steady slip (Fig. 3e–f; Chen et al., 2017 and Hrysiewicz, 2019), which is characterized by higher amplitude displacements. Regarding magnetic anomalies, the N65° structure is located above a large decrease in magnetization of 1000–3000 nT separating the high magnetic anomaly (> 2500 nT; Fig. 3g,h) into two branches: one occupying the northern part of the Grandes Pentes and the other the southern part. In the resistivity model of Dumont et al. (2019), a vertical discontinuity is visible in the western part of the N65° structure (lineament 2), while a strong vertical discontinuity delineates the north and southern blocks beneath lineament 3 at the eastern part of the N65° structure. In addition, the N65° structure separates an area of low S-wave velocity to the north from an area of higher S-wave velocity to the south (Fig. 3j; Mordret et al., 2015). The N65° structure is also associated with a strong decrease of the eruptive fissure density south of it, as shown in Fig. 3i, suggesting that it may represent a partial barrier to southward magma propagation that would explain the limited southward propagation of intrusion in the south flank compared the north flank. It is also noteworthy that the rupture area of the March–April 2007 co-eruptive slip modelled by Cayol et al. (2017) is located along the N65° structure, 0.5–1 km to the west of the V-shaped structure, indicating that the March–April 2007 slip may have been related to the N65° structure. Furthermore, the location of the March–April 2007 slip rupture corresponds to a zone of low seismicity between two major clusters to the east and west (Fig. 3j). Therefore, the three N65° lineaments observed in the morphology seems to correspond to the surface expression of a major structural discontinuity that divides the volcano into two distinct blocks characterized by different seismic velocities, different slip behaviours and different likelihood of eruptive activity. The northern sub-parallel branch of the N65° discontinuity (i.e. lineament 2) seems to be less significant but this may be an effect of our limited investigative resolution, which does not allow us to clearly distinguish its signature. This prevent us from distinguishing between the presence of two distinct discontinuities and a broad discontinuity zone encompassing both lineaments.

#### 5.1.2. The N120° structure

The second largest structure in terms of recurrence between the different datasets is the N120° lineament extending from the south-western edge of the summit cone to the southern base of the Grandes Pentes, further east (lineament 11 on Figs. 2 and 3). To the west, the N120° structure is associated with the sudden end of the summit cone, as indicated by a sharp slope change, and by the strong magnetic gradient delimiting the southern continuation of the summit positive magnetic anomaly (Fig. 3g,h). To the east, the structure delimits the southern part of both: (1) the slip area affecting the flank during the March–April 2007 co-eruptive, post-eruptive and steady state slip (Fig. 3a,f); and (2) the magnetized anomaly of the south-east flank. The N120° structure also appears to be in a zone of weak seismic activity (Fig. 3i). It can also be noted that, despite the decrease in eruptive fissure density south of the N65° discontinuity (lineaments 1–3), the activity going further south-east aligns along the N120° lineament (Fig. 3i), indicating either a channelling of intrusions along this direction or their stopping by encountering this structure. These observations support that the N120° structure is an important discontinuity delimiting a northern region corresponding to the most active zone of the volcano from a less active southern region.

#### 5.1.3. The chevron structures of the Grandes Pentes

In the Grandes Pentes area, four lineaments plus the easternmost termination of N65° discontinuity (3, 4, 5, 6, and 10) are arranged in a chevron pattern following N130–N160° and N50–80° orientations (Fig. 3). They are coincident with the eastern limit of the highly magnetized anomaly in the eastern flank (Fig. 3g,h), and delimit areas of different slip amplitude during co-eruptive slip displacements, during the March–April 2007 post-eruptive displacement and the long-term steady slip (Fig. 3c–f). We consider them as of secondary importance since they are associated with much weaker gradients and lower numbers of occurrences (Fig. 3k) in the different data types compared to the previous N65° and N120° discontinuities. They are also much shorter.

#### 5.1.4. Plaine des Osmondes structures

Finally, in the Plaine des Osmondes, three lineaments (7, 8, and 9) are associated with specific magnetic anomalies (Fig. 3g,h). The anomalies are quite large for the Plaine des Osmondes escarpments (lineaments 7 and 8) but much weaker for the last one farther east. In addition, the Plaine des Osmondes southern escarpment is associated with a seismic cluster elongated in the direction of the morphological and magnetic anomalies (lineament 8; Fig. 3i). We also note the presence of the N60–70° sharp decrease of eruptive fissure density coinciding in orientation with the southern escarpment (lineament 8), but shifted 500–1000 m south and west, lowering the confidence on any relation between both. Deformation measurement show no evidence of discontinuity in this area due to either a lack of surface deformation, the low quality of the measurement in this area (low InSAR coherence; Chen et al., 2017), or to the predominance of lava flow subsidence. We can however note that the resistivity model of Dumont et al. (2019) shows a sharp contrast in resistivity at the location of lineament 8.

### 5.2. Structure and mechanical behaviour of the eastern flank

This summary of observation highlights a network of discontinuities dissecting the eastern flank of Piton de la Fournaise volcano.

As almost all discontinuities can be observed in the co-eruptive and long-term displacements, the discontinuities (or at least their shallower part) should be located above the source of the displacements, thus, above the slip plane (independently of the slip mechanism; i.e. sheared sill or fault slip) determined by Dumont et al. (2022). This slip plane is suspected to be related to the presence of a sub-horizontal discontinuity guiding intrusion and locating slip around sea level (Dumont et al., 2022). In addition, Merle and Borgia (1996) have demonstrated that decollement planes such as the one evidence at the Piton de la Fournaise are likely to decouple the upper and lower part of volcanic edifices. Therefore, we suggest that these discontinuities actively affect a depth range starting from the near surface and extending from around sea level. Deeper continuation of the discontinuities cannot be ruled out but is less likely to have a major effect on the eastern flank dynamic. This shallow depth is also supported by the seismic velocities. The difference in S-wave velocity (≈5%–10%) between the north-west and south-east of the N65° discontinuity is only observed in the first hundred of meters below the surface (Mordret et al., 2015).

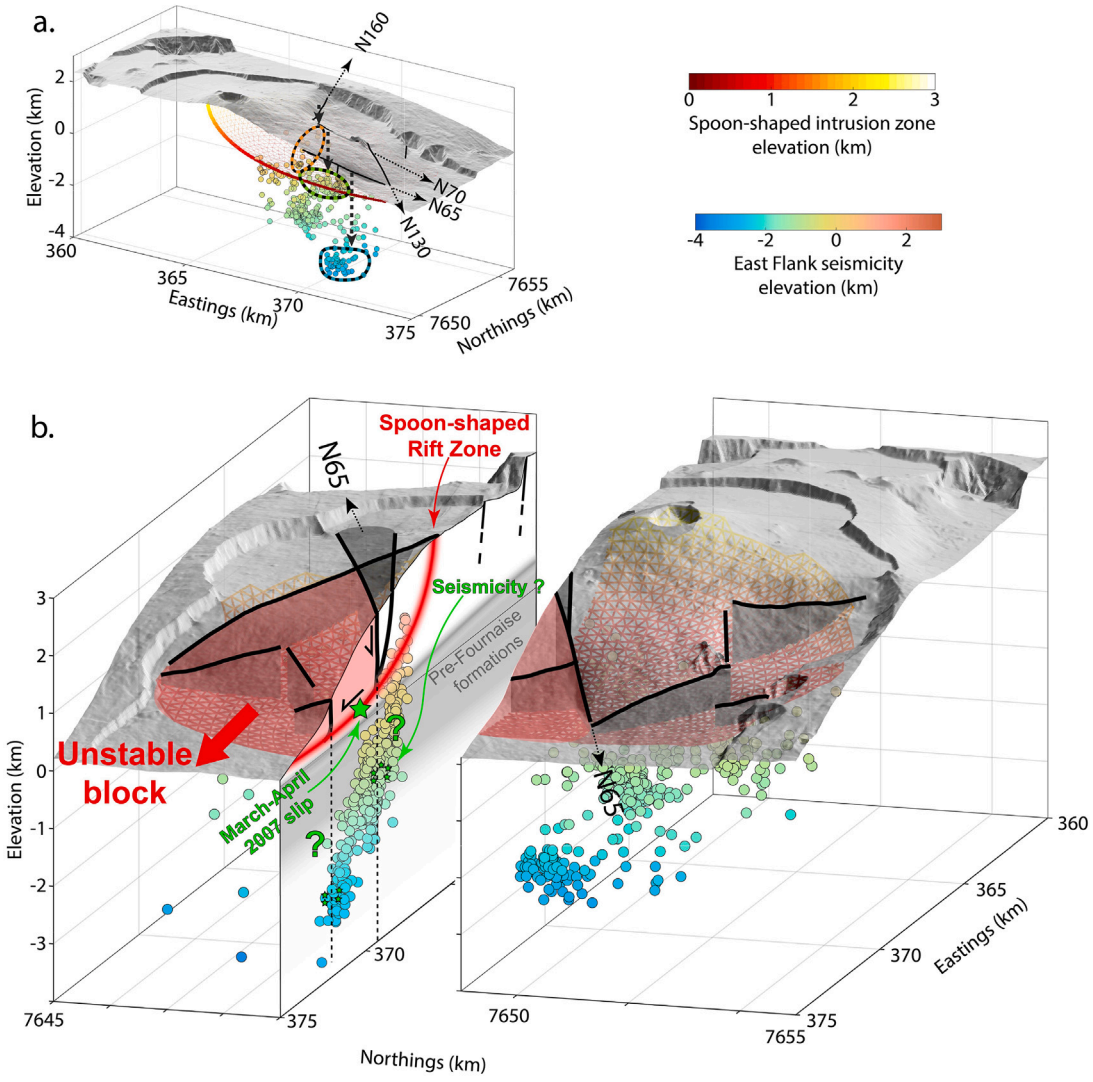


**Fig. 4. a.** 3D view of the link between seismicity clusters and lineaments with respect to depth. Orange, green and blue dashed contours highlight the cluster locations related to the N160°, N70° and N65°-V-shaped structure, respectively. The spoon-shaped intrusion zone is given as a triangular mesh for reference. **b.** gives the final interpretative 3D view of the lineaments location and depth in black (with potential deeper extent as dashed lines), together with the location of the unstable south-eastern block affected by long-term steady slip and sudden slip events, represented in red.

Furthermore, the sharp signal associated with the lineaments on the first vertical derivative of the magnetic map (Fig. 3h) also indicates the shallow nature of the structures causing the anomalies.

Separated by the N65° discontinuity, two main structural blocks, a north-western and a south-eastern, are observed (Fig. 3j). The north-western block is characterized by relatively low seismic velocities and affected by sheared sill intrusions. As sill intrusions are numerous in this area (six between 1998 and 2022; Dumont et al., 2022), the low seismic velocities may result from a higher temperature, a higher proportion of fluids and hydrothermalized formations or a higher degree of fracturing. However, this block does not show any pluriannual slow displacement (except for superficial subsidence due to thermo-mechanical contraction of the lava flows). The south-eastern block is decoupled from the rest of the edifice by the N65° and N120° discontinuities, and is affected by long-term steady slip and sudden slip events on a decollement fault plane (Tridon et al., 2016; Cayol et al., 2017; Dumont et al., 2022). This makes this structural block the most mobile of the edifice and therefore the main unstable sector of the volcano (Fig. 4). Both blocks should lie on the slip plane, at the base of the spoon-shaped intrusive structure.

### 5.3. Depth discrepancies between the discontinuities and the seismicity

The identified discontinuities, and thus the block limits, show a geographical coincidence with the seismic clusters beneath the eastern flank (Fig. 3i,j). Moreover, the seismicity also show a relation with the March–April 2007 slip event location, which corresponds to a low seismicity zone enclosed between two high seismicity zones to the west and east. This may indicate that the 2007 rupture corresponds to a zone of stress accumulation, which would be released sporadically during slip events. It should be noted, however, that the two high seismicity zones release stresses periodically, as “continuous” seismicity suggests, and not just during slip events. It is therefore tempting to consider that these relationships are not fortuitous and to attempt to link this seismicity to fracturing along the discontinuities.

However, despite the geographical coincidence (in map view) between the discontinuities, the 2007 rupture plane, and the seismicity, the depth of the seismic events (between +1 and −3 km above sea level) disagrees with the shallow depth of the modelled slip plane of the spoon-shaped structure (being between 0 and 500 m above sea level; Dumont et al., 2022) as well as the apparent superficiality of the discontinuities. If discontinuities extend deeper than the slip plane

and reach the depth of the seismic cluster to which they potentially correlate (Fig. 4a), it would suggest the presence of nearly vertical structures extending over 4 km depth in some locations. Vertical faults of this type are unlikely in such a volcanic context and on such a small geographic scale. Moreover, such vertical or sub-vertical faults would not explain why the distribution of the seismic clusters forms a plane inclined 45° to the east with a slight curvature in the north-south axis. The observed seismic surface is more likely to be encountered on a structure sharing these characteristics (eastward dip and north-south curvature) than on a network of vertical or sub-vertical faults. Spatial clustering is not explained either by the recently proposed triggering process of Gerbault et al. (2022), where the seismicity could results from the plastic shear-strain induced by the inflation of the magma chamber, located at sea level. Nor does this mechanism explain the temporal evolution of the seismicity rate, which increases during the propagation of intrusions within the rift zones (Gerbault et al., 2022; OVPF, 2020). An alternative triggering mechanism for the seismicity was proposed by Dumont et al. (2024). They showed that intrusive activity increases the Coulomb stress both on the seismogenic plane beneath the eastern flank and at the base of the potentially seismogenic spoon-shaped structure. Rift zone activity is a more likely source, as it induces deformation one or two orders of magnitude greater than reservoir inflation and it is consistent with the temporal evolution of the seismicity rate. However, this does not explain the clustering either and would result in a cup-shaped shear-strain zone, slightly shallower than with the reservoir inflation, favouring seismicity slightly closer to sea level. It is therefore not easy to reconcile these observations (fracturing and seismicity) without pointing to uncertainties, either in the depth of the discontinuities or in the depth of the earthquakes.

On the one hand, the location of seismicity at depth could be altered by an inappropriate velocity model. The model used by OVPF is a 1D velocity gradient following the topography (P wave velocity of 3.3 km/s at free surface and increasing by 0.3 km/s per kilometer; Duputel et al., 2021), which was fitted for the summit region (Prôno et al., 2009). Velocities could be lower than expected by this model, especially in the first kilometer below the surface, as suggested by the shear wave velocity model found by Mordret et al. (2015), which would results in P-wave velocity lower by ≈1 km/s (velocity models comparison can be found in Supplementary Material S11). Moreover, the eastern flank may be more fractured than assumed, as shown by the numerous discontinuities we have highlighted here. We also know that the east flank is partly made up of formations with low seismic velocities, as suggested by the presence of hydrothermalized formations and hyaloclastites in the Grand Brûlé borehole (Rançon et al., 1989), or even fluvial deposits (Courteaud, 1996), as well as gabbroic formations whose velocities have recently been shown to be particularly low even in dry condition (down to 1.9 km/s; Di Muro et al., 2021). Such lower velocities would lead to shallower events locations. On the other hand, inverse deformation models were conducted assuming a homogeneous crust. However, it is well known that the crust is layered with lower velocities at lower elevations. Taking this layering into account in the inversions, could lead to deeper locations of the sills, sheared sills and faults at the base of the spoon-shaped structure (Montgomery-Brown et al., 2009), but it is unlikely these locations reach a few kilometers below sea level.

Additional research is required to resolve this inconsistency. Deformation modelling that accounts for heterogeneity, together with hypocenter relocations on the eastern flank and focal mechanism determination, would refine the geometry of the structures and clarify their relationships, potentially revealing their alignment (Fig. 4).

### 5.4. Implications for the origin of the discontinuities

The two families of discontinuities identified above show N50–80° and N120–160° directions. Structures with such orientations may have several origins, from large-scale crustal influences to local intra-edifice influences, such as the stress field or magmatic activity and its evolution over time. In a previous island-scale synthetic study, Michon et al. (2007) showed that structures with N70–80° directions and few with N120° directions can be found outside the caldera, and on the eastern submarine flank of the island based on morphological evidence, local crustal fabrics and inverse magnetic anomaly. It is assumed that these structures probably resulted from a regional structural control. However, some structures trending N140–160°, found only locally in the southern flank of Piton de la Fournaise, have been interpreted as of local origin.

Here, the discontinuities we describe seem to be restricted to the eastern flank of Piton de la Fournaise and within the caldera limits, despite the high resurfacing rate by lava flows within the Enclos Fouqué. This observation reinforces confidence in their local presence, exclusively. The same is observed for magnetic data where no significant anomaly presenting similar characteristics as within the caldera, are observed outside the caldera (see Supplementary Material). Similarly, seismicity of the eastern flank also seems to be limited to the inner part of the caldera (Duputel et al., 2021). The Enclos Fouqué caldera appears to be the boundary delimiting the extent of most of the discontinuities and seismicity, as well as of 97% of the eruptive activity (Lénat and Bachèlery, 1988; Stieltjes and Moutou, 1989). It is therefore likely for the discontinuities of the eastern flank to have a local origin either inherited from the formation of the Enclos Fouqué, or generated by process(es) restricted to the Enclos Fouqué, such as the magmatic activity and/or the east–west extension by the slow creep of the eastern flank. Such local origin would also agree with the apparent shallowness of the discontinuities.

Regarding the N65° discontinuity, Michon and Saint-Ange (2008) proposed to interpret it as a normal fault accommodating the subsidence of Les Alizés hypovolcanic complex located further east. This categorization as a fault is in agreement with the geophysical observations (delimitation of the long-term flank slip sector, local shallow demagnetization). In the Michon and Saint-Ange (2008) hypothesis, the fault created by Les Alizés subsidence could decouple a part of the edifice and could then explain the difference in slip behaviour we observe to the north-west and south-east of the fault. Similarly, the fault would also accommodate the east–west extension resulting from the steady state slip of the flank. Conversely, the difference in slip behaviour between the north-western and south-eastern zones could be responsible for the decoupling of the edifice into two main blocks and the creation/enhancement of the fault. In this framework, the difference in slip behaviour could result from differences in friction properties. Such differences could be explained by the spatial distribution of low friction formations related to hyaloclastites or Les Alizés intrusive body (unconstrained under the Grandes Pentes). Indeed, Di Muro et al. (2021) have shown by experimental tests that the gabbro of the intrusive complex could localize the deformation and creep and represent a potential slip surface. It is likely that Les Alizés intrusive complex has a major influence on the slip and seismic behaviour, and potentially on the formation/enhancement of the fault. Further work focusing on a better characterization of the spatial location of the intrusive complex and on the effect of the spatial distribution of friction properties on strain localization would clarify the eastern flank dynamic.

### 5.5. Implications for further investigations and hazards assessments

Regardless of their origin, the N65° and N120° discontinuities play a major role in accommodating south-eastern flank slip, as shown by the long-term flank displacements accumulating strain along them. Because the N65° and N120° discontinuities enclose the most unstable sector of the volcano flank (Fig. 4b), the interaction between these discontinuities, the intrusive activity and the slip plane could result in major earthquakes in the long term. Similar interactions have been observed at Mount Etna, where earthquakes on a network of border

faults and flank slip are triggered by magmatic activity (Acocella et al., 2003; Puglisi et al., 2008; Azzaro et al., 2013, 2020; Iozzia et al., 2024). At Etna, the location of the border fault is however clearer than at Piton de la Fournaise and outlined by the geology, seismotectonics, and slip rates. At this volcano, five kinematic domains are defined (Azzaro et al., 2020) and the main structures can be followed offshore of the continental margin (Urlaub et al., 2022). Only two blocks can be defined at Piton de la Fournaise, and no continuation of the structures are found outside the caldera nor offshore. At Piton de la Fournaise, only the silent fault slip events we have described were highlighted (Dumont et al., 2022), corresponding to a moment magnitude of $M_W$ = 4.4 - 4.6, but no large flank earthquakes has been reported since the beginning of the monitoring (1980). We cannot rule out the possibility that an earthquake of such magnitude or greater could occur due to the continuous stress build up induced by intrusions (Dumont et al., 2024). Such an earthquake could trigger a tsunami or a large flank collapse (whether the whole flank or the area restricted to the south-east of the N65° discontinuity). More needs to be known about the geometry of the discontinuities and their seismogenic potential, as well as their relationship with the basal slip plane.

## 6. Conclusion

Based on several independent datasets including, seismicity, deformation, magnetic anomalies, and eruptive fissure density, we have analysed a set of morphological lineaments highlighted in the eastern flank of Piton de la Fournaise volcano. The consistency of the locations and orientations of the surface lineaments and the strong gradients in the geophysical data confirm that the lineaments detected in the morphology are the surface expression of structural discontinuities affecting the internal part of the volcano. Overall, the different discontinuities evidence a network of intersecting structures in the Grandes Pentes following two main orientations: a family striking N50–80° and a family striking N120–160°. They delimit blocks and sub-blocks, each having a differential movement with respect to the others. The spatial distribution of the discontinuities, which are not present outside the caldera, suggests that they results from local processes, such as intra-caldera processes or the formation of the Enclos Fouqué caldera itself.

Among these discontinuities, a major discontinuity striking N65° that runs through the middle of the eastern flank divides the edifice into two major blocks: (1) a north-western block with low seismic velocity and only co-intrusive slip on sheared sills; (2) a south-eastern block with higher seismic velocity and slip on a fault plane, whose activity continues over the long term, likely drive by slow creep. Both blocks probably lie on the sub-horizontal base of a spoon-shaped destabilization structure located around sea level. The reason leading to the coexistence of two different slip behaviours (sheared sills and fault slip) is unclear. It could be caused by the spatial distribution of different friction properties, due to the presence of the intrusive body of Les Alizés for example, then creating a decoupling of the edifice along the N65° discontinuity. Conversely, the pre-existing presence of the discontinuity could decouple the edifice resulting in a different slip behaviour in the south-east part.

To better characterize the structure and functioning of the eastern flank, two major questions that remain unanswered should be further investigated. First, it seems necessary to better constrain the depth of different structures and lithologies identified beneath the eastern flank. Especially, concerning the eastern flank seismicity and its relationship with the above spoon-shaped structure and discontinuities. Event relocations and focal mechanisms appear necessary to better understand the geometry of the seismogenic structure and the mechanism of their fracturing. Second, greater attention should be given to the origins of the two distinct slip mechanism by clarifying the location and influence of Les Alizés complex or by testing the effect of different friction properties on strain localization.

Relations between the spoon-shaped destabilization structure, the two slip behaviours, the discontinuities and the seismicity is a major parameter to consider in estimating the stability of the eastern flank and the associated hazards in terms of seismicity or flank failure potentially leading to tsunamis. Indeed, the discontinuities, and particularly the major N65° one, could be seismogenic and/or could delimit a potential destabilization zone in a flank collapse, which would then be more restricted than in the case of a total destabilization of the spoon-shaped structure. Such alternative flank failure scenario should be accounted for future for flank failure and tsunami hazard assessment.

## CRediT authorship contribution statement

**Quentin Dumont:** Writing – review & editing, Writing – original draft, Visualization, Validation, Methodology, Investigation, Formal analysis, Conceptualization. **Jean-Luc Froger:** Writing – review & editing, Writing – original draft, Data curation. **Marc Dumont:** Writing – review & editing, Writing – original draft, Data curation. **Lydie Gailler:** Writing – review & editing, Writing – original draft, Validation. **Patrick Bachèlery:** Writing – review & editing, Writing – original draft, Validation. **Valérie Cayol:** Writing – review & editing, Writing – original draft, Validation, Software.

## Declaration of competing interest

The authors declare the following financial interests/personal relationships which may be considered as potential competing interests: Valerie Cayol reports financial support was provided by National Centre for Scientific Research. If there are other authors, they declare that they have no known competing financial interests or personal relationships that could have appeared to influence the work reported in this paper.

## Acknowledgements

This work was supported by the TelluS program of CNRS/INSU, by the EUROVOLC project, under the EU Horizon 2020 Research and Innovation Action, grant No. 731070. This research was financed by the French Government Laboratory of Excellence initiative no. ANR-10-LABX-0006, the Region Auvergne and the European Regional Development Fund. This is Laboratory of Excellence ClerVolc contribution number 750. The present study was financially supported by the Japan Society for the Promotion of Science (JSPS) within the JSPS International Fellowships for Research in Japan program. InSAR data were acquired within the framework of the Indian Ocean InSAR Observatory (OI2/ISDeform/INSU). The seismic location data were determined by the Observatoire Volcanologique du Piton de la Fournaise/Institut de Physique du Globe de Paris (OVPF/IPGP). The magnetic data were obtained and are the propriety of the Bureau de Recherches Géologiques et Minières (Banque de Données Aérogéophysiques de France – LICENCE n°2021/011 - BRGM, 2021).

## Appendix A. Supplementary data

Supplementary material related to this article can be found online at https://doi.org/10.1016/j.jvolgeores.2026.108579.

## Data availability

Data will be made available on request.

## References


Acocella, V., Behncke, B., Neri, M., D'Amico, S., 2003. Link between major flank slip 2002–2003 eruption at Mt. Etna (Italy). Geophys. Res. Lett. 30 (24), 10–13. http://dx.doi.org/10.1029/2003GL018642.

Adler, P.M., Mouel, J.l.L., Zlotnicki, J., 1999. Electrokinetic and magnetic fields generated by flow through a fractured zone: a sensitivity study for La Fournaise volcano. Geophys. Res. Lett. 26 (6), 795–798.

Azzaro, R., Bonforte, A., Amico, S.D., Guglielmino, F., Scarfì, L., 2020. Stick-slip vs stable sliding fault behaviour: A case-study using a multidisciplinary approach in the volcanic region of Mt . Etna ( Italy ). Tectonophysics 790 (June), 228554. http://dx.doi.org/10.1016/j.tecto.2020.228554.

Azzaro, R., Bonforte, A., Branca, S., Guglielmino, F., 2013. Geometry and kinematics of the fault systems controlling the unstable fl ank of Etna volcano (Sicily). J. Volcanol. Geotherm. Res. 251, 5–15. http://dx.doi.org/10.1016/j.jvolgeores.2012.10.001.

Bachèlery, P., 1981. Le Piton de la Fournaise (Ile de la Reunion). Etude volcanologique, structurale et petrologique. Piton de la Fournaise, Reunion; volcanologic, structural and petrographic study (Ph.D. thesis). Univ. of Clermont-Ferrand, p. 255.

Bachèlery, P., Mairine, P., 1990. Evolution volcano-structurale du Piton de la Fournaise depuis 0.53 Ma. In: Le volcanisme de la Réunion, Monographie.

Baranov, V., 1957. A new method for interpretation of aeromagnetic maps: pseudo-gravimetric anomalies. Geophysics XXII (2).

Barde-Cabusson, S., Finizola, A., Peltier, A., Chaput, M., Taquet, N., Dumont, S., Duputel, Z., Guy, A., Mathieu, L., Saumet, S., Sorbadère, F., Vieille, M., 2012. Structural control of collapse events inferred by self-potential mapping on the piton de la fournaise volcano (La Réunion Island). J. Volcanol. Geotherm. Res. 209–210, 9–18. http://dx.doi.org/10.1016/j.jvolgeores.2011.09.014.

Battaglia, J., Ferrazzini, V., Staudacher, T., Aki, K., Cheminée, J.L., 2005. Pre-eruptive migration of earthquakes at the piton de la fournaise volcano (Réunion Island). Geophys. J. Int. 161 (2), 549–558. http://dx.doi.org/10.1111/j.1365-246X.2005.02606.x.

Beauducel, F., Peltier, A., Villié, A., Suryanto, W., 2020. Mechanical imaging of a volcano plumbing system from GNSS unsupervised modeling. Geophys. Res. Lett. 47 (17), http://dx.doi.org/10.1029/2020GL089419.

Berthod, C., Famin, V., Bascou, J., Michon, L., Ildefonse, B., Monié, P., 2016. Evidence of sheared sills related to flank destabilization in a basaltic volcano. Tectonophysics 674, 195–209. http://dx.doi.org/10.1016/j.tecto.2016.02.017.

Bonali, F.L., Corazzato, C., Tibaldi, A., 2011. Identifying rift zones on volcanoes: An example from La Réunion island, Indian ocean. Bull. Volcanol. 73 (3), 347–366. http://dx.doi.org/10.1007/s00445-010-0416-1.

Bonforte, A., Guglielmino, F., Coltelli, M., Ferretti, A., Puglisi, G., 2011. Structural assessment of mount etna volcano from permanent scatterers analysis. Geochem. Geophys. Geosyst. 12 (2), http://dx.doi.org/10.1029/2010GC003213.

Boudoire, G., Liuzzo, M., Di Muro, A., Ferrazzini, V., Michon, L., Grassa, F., Derrien, A., Villeneuve, N., Bourdeu, A., Brunet, C., Giudice, G., Gurrieri, S., 2017. Investigating the deepest part of a volcano plumbing system: Evidence for an active magma path below the western flank of Piton de la Fournaise (La Réunion Island). J. Volcanol. Geotherm. Res. 341, 193–207. http://dx.doi.org/10.1016/j.jvolgeores.2017.05.026.

Bouligand, C., Hurwitz, S., Vandemeulebrouck, J., Byrdina, S., Kass, M.A., Lewicki, J.L., 2019. Heat and mass transport in a vapor-dominated hydrothermal area in Yellowstone National Park, USA : Inferences from magnetic, electrical, electromagnetic, subsurface temperature, and diffuse CO2 flux measurements. J. Geophys. Res. : Solid Earth 124, 291–309. http://dx.doi.org/10.1029/2018JB016202.

Camacho, A.G., Fernández, J., Samsonov, S.V., Tiampo, K.F., Palano, M., 2020. 3D multi-source model of elastic volcanic ground deformation. Earth Planet. Sci. Lett. 547, 116445. http://dx.doi.org/10.1016/j.epsl.2020.116445.

Cayol, V., Tridon, M., Froger, J.-L., Augier, A., Bachèlery, P., 2017. Inversion of coeval shear and normal stress of piton de la fournaise flank displacement. In: IAVCEI 2017 Scientific Assembly, Forstering Integrative Studies of Volcanoes. p. 180, URL http://iavcei2017.org.

Chaput, M., Famin, V., Michon, L., 2017. Sheet intrusions and deformation of Piton des Neiges, and their implication for the volcano-tectonics of La Réunion. Tectonophysics 717.

Chaput, M., Pinel, V., Famin, V., Michon, L., Froger, J.-L., 2014. Cointrusive shear displacement by sill intrusion in a detachment: A numerical approach. Geophys. Res. Lett. 41 (9), 3307–3314. http://dx.doi.org/10.1002/2014GL061184.Received.

Chen, Y., Remy, D., Froger, J.L., Peltier, A., Villeneuve, N., Darrozes, J., Perfettini, H., Bonvalot, S., 2017. Long-term ground displacement observations using InSAR and GNSS at piton de la fournaise volcano between 2009 and 2014. Remote Sens. Environ. 194 (March 1998), 230–247. http://dx.doi.org/10.1016/j.rse.2017.03.038.

Courteaud, M., 1996. Étude des structures géologiques et hydrogéologiques du massif de la Fournaise par la méthode audiomagnétotellurique (Ph.D. thesis). Université de la Réunion, URL http://www.theses.fr/1996LARES004.

Delaney, P.T., Pollard, D.D., Ziony, I., Mckee, E.H., 1986. Field relations between dikes and joints: Emplacement processes and paleostress analysis. J. Geophys. Res. 91 (5), 4920–4938.

Denlinger, R.P., Morgan, J.K., 2014. Instability of hawaiian volcanoes. U.S. Geol. Surv. Prof. Pap. 1801 148–177.

Di Muro, A., Schwarzlmueller, F., Kueppers, U., Heap, M., Dingwell, D.B., 2021. Petrophysical characterisation of volcanic ejecta to constrain subsurface lithological heterogeneities: implications for edifice stability at basaltic volcanoes. Volcanica 4, 41–66. http://dx.doi.org/10.30909/vol.04.01.4166.

Drymoni, K., Browning, J., Gudmundsson, A., 2021. Volcanotectonic interactions between inclined sheets, dykes, and faults at the Santorini Volcano, Greece. J. Volcanol. Geotherm. Res. 416, 107294. http://dx.doi.org/10.1016/j.jvolgeores.2021.107294.

Duffield, W.A., Stieltjes, L., Varet, J., 1982. Huge landslide blocks in the growth of Piton de la Fournaise, La Réunion, and Kilauea volcano, Hawaii. J. Volcanol. Geotherm. Res. 12 (1–2), 147–160. http://dx.doi.org/10.1016/0377-0273(82)90009-9.

Dumont, Q., Cayol, V., Froger, J.L., 2021. Mitigating bias in inversion of InSAR data resulting from radar viewing geometries. Geophys. J. Int. 227 (1), 483–495. http://dx.doi.org/10.1093/gji/ggab229.

Dumont, Q., Cayol, V., Froger, J.l., 2024. Is stress modeling able to forecast intrusions and slip events at Piton de la Fournaise volcano ? Earth Planet. Sci. Lett. 626 (March 2023), 118494. http://dx.doi.org/10.1016/j.epsl.2023.118494.

Dumont, Q., Cayol, V., Froger, J.L., Peltier, A., 2022. 22 years of satellite imagery reveal a major destabilization structure at Piton de la Fournaise. Nat. Commun. 13, 1–11. http://dx.doi.org/10.1038/s41467-022-30109-w.

Dumont, M., Peltier, A., Roblin, E., Reninger, P.A., Barde-Cabusson, S., Finizola, A., Ferrazzini, V., 2019. Imagery of internal structure and destabilization features of active volcano by 3D high resolution airborne electromagnetism. Sci. Rep. 9 (1), 1–11. http://dx.doi.org/10.1038/s41598-019-54415-4.

Dumont, M., Reninger, P.A., Aunay, B., Pryet, A., Jougnot, D., Join, J.L., Michon, L., Martelet, G., 2021. Hydrogeophysical characterization in a volcanic context from local to regional scales combining airborne electromagnetism and magnetism. Geophys. Res. Lett. 48 (12), http://dx.doi.org/10.1029/2020GL092000.

Duncan, R.A., Backman, J., Peterson, L., 1989. Reunion hotspot activitity through tertiary time: Initial results from the ocean drilling program, leg 115. J. Volcanol. Geotherm. Res. 36 (1–3), 193–198. http://dx.doi.org/10.1016/0377-0273(89)90013-9.

Duputel, Z., Ferrazzini, V., Lengliné, O., Michon, L., Fontaine, F.R., Massin, F., 2021. Seismicity of La Réunion island. C. R. Géosci. 0–19.

Elkins, T.A., 1951. The second derivative method of gravity interpretation. Annu. Meet. Soc. Explor. Geophys.

Famin, V., Berthod, C., Michon, L., Eychenne, J., Brothelande, E., Mahabot, M.M., Chaput, M., 2016. Localization of magma injections, hydrothermal alteration, and deformation in a volcanic detachment (Piton des Neiges, La Réunion). J. Geodyn. 101, 155–169. http://dx.doi.org/10.1016/j.jog.2016.05.007.

Famin, V., Michon, L., 2010. Volcano destabilization by magma injections in a detachment. Geology 38 (3), 219–222. http://dx.doi.org/10.1130/G30717.1.

Fitterman, D.V., 1979. Theory of electrokinetic-magnetic anomalies in a faulted half-space. J. Geophys. Res. 84 (9), 6031–6040.

Froger, J.L., Famin, V., Cayol, V., Augier, A., Michon, L., Lénat, J.F., 2015. Time-dependent displacements during and after the April 2007 eruption of Piton de la Fournaise, revealed by interferometric data. J. Volcanol. Geotherm. Res. 296 (April 2007), 55–68. http://dx.doi.org/10.1016/j.jvolgeores.2015.02.014.

Fukushima, Y., Cayol, V., Durand, P., 2005. Finding realistic dike models from interferometric synthetic aperture radar data: The february 2000 eruption at Piton de la Fournaise. J. Geophys. Res. B: Solid Earth 110 (3), 1–15. http://dx.doi.org/10.1029/2004JB003268.

Fukushima, Y., Cayol, V., Durand, P., Massonnet, D., 2010. Evolution of magma conduits during the 1998–2000 eruptions of Piton de la Fournaise volcano, Réunion Island. J. Geophys. Res.: Solid Earth 115 (10), http://dx.doi.org/10.1029/2009JB007023.

Gailler, L., Kauahikaua, J., 2017. Monitoring the cooling of the 1959 kīlauea iki lava lake using surface magnetic measurements. Bull. Volcanol. 1–7. http://dx.doi.org/10.1007/s00445-017-1119-7.

Gailler, L.S., Lénat, J.F., 2012. Internal architecture of La Réunion (Indian ocean) inferred from geophysical data. J. Volcanol. Geotherm. Res. 221–222, 83–98. http://dx.doi.org/10.1016/j.jvolgeores.2012.01.015.

Gailler, L.S., Lénat, J.F., Lambert, M., Levieux, G., Villeneuve, N., Froger, J.L., 2009. Gravity structure of Piton de la Fournaise volcano and inferred mass transfer during the 2007 crisis. J. Volcanol. Geotherm. Res. 184 (1–2), 31–48. http://dx.doi.org/10.1016/j.jvolgeores.2009.01.024.

Gailler, L.S., Martí, A., Lénat, J.F., 2018. Complex structure of Piton de la Fournaise and its underlying lithosphere revealed by magnetotelluric 3D inversion. J. Volcanol. Geotherm. Res. 356, 200–210. http://dx.doi.org/10.1016/j.jvolgeores.2018.03.006.

Gerbault, M., Fontaine, F.J., Peltier, A., Got, J.L., Hassani, R., Ferrazzini, V., Gailler, L., Duputel, Z., 2022. What causes the persistent seismicity below the eastern flank of Piton de la Fournaise (la Réunion Island)? Elasto-plastic models of magma inflation. J. Volcanol. Geotherm. Res. 431 (March), 107628. http://dx.doi.org/10.1016/j.jvolgeores.2022.107628.

Gillot, P.Y., Lefèvre, J.C., Nativel, P.E., 1994. Model for the structural evolution of the volcanoes of Réunion Island. Earth Planet. Sci. Lett. 122 (3–4), 291–302. http://dx.doi.org/10.1016/0012-821X(94)90003-5.

Hrysiewicz, A., 2019. Caractérisation des déplacements liés aux coulées de lave au Piton de la Fournaise à partir de données InSAR (Ph.D. thesis). Université Clermont Auvergne.

Iozzia, A., Currenti, G., Cayol, V., Bonforte, A., Cannata, A., Froger, J.L., 2024. Mechanically consistent model of the 2018 christmas volcano-tectonic event at Etna. Geophys. Res. Lett. 51 (14), 1–11. http://dx.doi.org/10.1029/2023GL108017.

Kelfoun, K., Giachetti, T., Labazuy, P., 2010. Landslide-generated tsunamis at Réunion Island. J. Geophys. Res.: Earth Surf. 115 (4), 1–17. http://dx.doi.org/10.1029/2009JF001381.

Labazuy, P., 1996. Recurrent landslide events on the submarine flank of the Piton de la Fournaise volcano (Réunion Island. Volcano Instab. Earth Other Planets 110 (110), 295–306.

Lénat, J.F., Bachèlery, P., 1988. Dynamics of magma transfer at Piton de la Fournaise Volcano (Réunion Island, Indian ocean). In: Verlag., W.V.T. (Ed.), Modeling of Volcanic Processes. pp. 57–72.

Lénat, J.F., Bachèlery, P., Merle, O., 2012a. Anatomy of Piton de la Fournaise volcano (La Réunion, Indian ocean). Bull. Volcanol. 74 (9), 1945–1961. http://dx.doi.org/10.1007/s00445-012-0640-y.

Lénat, J.F., Bachèlery, P., Peltier, A., 2012b. The interplay between collapse structures, hydrothermal systems, and magma intrusions: The case of the central area of Piton de la Fournaise volcano. Bull. Volcanol. 74 (2), 407–421. http://dx.doi.org/10.1007/s00445-011-0535-3.

Lénat, J.F., Fitterman, D., Jackson, D.B., Bachèlery, P., 2000. Structure and dynamics of the central zone of Piton de la Fournaise volcano. Bull. Volcanol. 62, 75–89.

Lénat, J.F., Vincent, P., Bachélery, P., 1989. The off-shore continuation of an active basaltic volcano: Piton de la fournaise (réunion island, Indian ocean); structural and geomorphological interpretation from sea beam mapping. J. Volcanol. Geotherm. Res. 36 (1–3), http://dx.doi.org/10.1016/0377-0273(89)90003-6.

Lengliné, O., Duputel, Z., Ferrazzini, V., 2016. Uncovering the hidden signature of a magmatic recharge at Piton de la Fournaise volcano using small earthquakes. Geophys. Res. Lett. 43 (9), 4255–4262. http://dx.doi.org/10.1002/2016GL068383.

Malengreau, B., Lénat, J.F., Froger, J.L., 1999. Structure of réunion island (Indian ocean) inferred from the interpretation of gravity anomalies. J. Volcanol. Geothennal Res. 88, 131–146.

Martelet, G., Reninger, P.A., Perrin, J., Deparis, J., 2014. Acquisition géophysique héliportée de l'île de La Réunion. Technical Report, BRGM.

Martínez-Poza, A.I., Druguet, E., Castaño, L.M., Carreras, J., 2014. Dyke intrusion into a pre-existing joint network: The Aiguablava lamprophyre dyke swarm (Catalan Coastal ranges). Tectonophysics 630 (C), 75–90. http://dx.doi.org/10.1016/j.tecto.2014.05.015.

Merle, O., Borgia, A., 1996. Scaled experiments of volcanic spreading. J. Geophys. Res.: Solid Earth 101 (B6), 13805–13817. http://dx.doi.org/10.1029/95jb03736.

Merle, O., Lénat, J.F., 2003. Hybrid collapse mechanism at Piton de la Fournaise volcano, Reunion Island, Indian ocean. J. Geophys. Res.: Solid Earth 108 (B3), 1–11. http://dx.doi.org/10.1029/2002jb002014.

Merle, O., Mairine, P., Michon, L., Bachèlery, P., Smietana, M., 2010. Calderas, landslides and paleo-canyons on Piton de la Fournaise volcano (La Réunion Island, Indian ocean). J. Volcanol. Geotherm. Res. 189 (1–2), 131–142. http://dx.doi.org/10.1016/j.jvolgeores.2009.11.001.

Michon, L., Cayol, V., Letourneur, L., Peltier, A., Villeneuve, N., Staudacher, T., 2009. Edifice growth, deformation and rift zone development in basaltic setting: Insights from Piton de la Fournaise shield volcano (Réunion Island). J. Volcanol. Geotherm. Res. 184 (1–2), 14–30. http://dx.doi.org/10.1016/j.jvolgeores.2008.11.002.

Michon, L., Ferrazzini, V., Di Muro, A., Villeneuve, N., Famin, V., 2015. Rift zones and magma plumbing system of Piton de la Fournaise volcano: How do they differ from Hawaii and Etna? J. Volcanol. Geotherm. Res. 303, 112–129. http://dx.doi.org/10.1016/j.jvolgeores.2015.07.031.

Michon, L., Lénat, J.f., Bachèlery, P., Di Muro, A., 2016. Geology and morphostructural evolution of Piton de la Fournaise. In: Active Volcanoes of the Southwest Indian Ocean: Piton de la Fournaise and Karthala. pp. 45–59.

Michon, L., Saint-Ange, F., 2008. Morphology of Piton de la Fournaise basaltic shield volcano (La Réunion Island): Characterization and implication in the volcano evolution. J. Geophys. Res.: Solid Earth 113 (3), 1–19. http://dx.doi.org/10.1029/2005JB004118.

Michon, L., Saint-Ange, F., Bachèlery, P., Villeneuve, N., Staudacher, T., 2007. Role of the structural inheritance of the oceanic lithosphere in the magmato-tectonic evolution of Piton de la Fournaise volcano (La Runion island). J. Geophys. Res.: Solid Earth 112 (4), 1–21. http://dx.doi.org/10.1029/2006JB004598.

Mohamed-Abchir, A., 1996. Les cendres de bellecombe (cb) : un evenement explosif majeur dans le passe recent du piton de la fournaise, ile de la reunion (Ph.D. thesis). Paris 7.

Montgomery-Brown, E.K., Segall, P., Miklius, A., 2009. Kilauea slow slip events: Identification, source inversions, and relation to seismicity. J. Geophys. Res. 114 (June), 1–20. http://dx.doi.org/10.1029/2008jb006074.

Mordret, A., Rivet, D., Landès, M., Shapiro, N.M., 2015. Three-dimensional shear velocity anisotropic model of Piton de la Fournaise Volcano (La Réunion Island) from ambient seismic noise. J. Geophys. Res.: Solid Earth 120 (1), 406–427. http://dx.doi.org/10.1002/2014JB011654.

Nakamura, K., 1977. Volcanoes as possible indicators of tectonic stress orientation - principle and proposal. J. Volcanol. Geotherm. Res. 2 (1), 1–16. http://dx.doi.org/10.1016/0377-0273(77)90012-9.

Oehler, J.F., Labazuy, P., Lénat, J.F., 2004. Recurrence of major flank landslides during the last 2-ma-history of Reunion Island. Bull. Volcanol. 66 (7), 585–598. http://dx.doi.org/10.1007/s00445-004-0341-2.

Oehler, J.F., Lénat, J.F., Labazuy, P., 2008. Growth and collapse of the Reunion Island volcanoes. Bull. Volcanol. 70 (6), 717–742. http://dx.doi.org/10.1007/s00445-007-0163-0.

Ort, M.H., Di Muro, A., Michon, L., Bachèlery, P., 2016. Explosive eruptions from the interaction of magmatic and hydrothermal systems during flank extension: the bellecombe tephra of Piton de La Fournaise (La Réunion Island). Bull. Volcanol. 78 (1), 1–14. http://dx.doi.org/10.1007/s00445-015-0998-8.

OVPF, 2020. Bulletin mensuel de l'Observatoire Volcanologique du Piton de la Fournaise. Technical Report September, IPGP, URL http://www.ipgp.fr/fr/ovpf/bulletin-mensuel-lundi-5-octobre-2020.

Palano, M., 2016. Episodic slow slip events and seaward flank motion at Mt. Etna volcano (Italy). J. Volcanol. Geotherm. Res. 324, 8–14. http://dx.doi.org/10.1016/j.jvolgeores.2016.05.010.

Peltier, A., Bachèlery, P., Staudacher, T., 2009. Magma transport and storage at Piton de La Fournaise (La Réunion) between 1972 and 2007: A review of geophysical and geochemical data. J. Volcanol. Geotherm. Res. 184 (1–2), 93–108. http://dx.doi.org/10.1016/j.jvolgeores.2008.12.008.

Peltier, A., Beauducel, F., Villeneuve, N., Ferrazzini, V., Di Muro, A., Aiuppa, A., Derrien, A., Jourde, K., Taisne, B., 2016. Deep fluid transfer evidenced by surface deformation during the 2014–2015 unrest at Piton de la Fournaise volcano. J. Volcanol. Geotherm. Res. 321, 140–148. http://dx.doi.org/10.1016/j.jvolgeores.2016.04.031.

Peltier, A., Got, J.l., Villeneuve, N., Boissier, P., Staudacher, T., Ferrazzini, V., Walpersdorf, A., 2015a. Long-term mass transfer at Piton de la Fournaise volcano evidenced by strain distribution derived from GNSS network. J. Geophys. Res.: Solid Earth 120, 1874–1889. http://dx.doi.org/10.1002/2015JB012664.Received.

Peltier, A., Poland, M.P., Staudacher, T., 2015b. Are Piton de la Fournaise (La Réunion) and Kilauea (Hawai'i) really "analog volcanoes"? Am. Geophys. Union Monogr. 208, 507–531. http://dx.doi.org/10.1002/9781118872079.ch23.

Poland, M.P., Peltier, A., Bonforte, A., Puglisi, G., 2017. The spectrum of persistent volcanic flank instability: A review and proposed framework based on Kīlauea, Piton de la Fournaise, and Etna. J. Volcanol. Geotherm. Res. 339, 63–80. http://dx.doi.org/10.1016/j.jvolgeores.2017.05.004.

Prôno, E., Battaglia, J., Monteiller, V., Got, J.L., Ferrazzini, V., 2009. P-wave velocity structure of Piton de la Fournaise volcano deduced from seismic data recorded between 1996 and 1999. J. Volcanol. Geotherm. Res. 184 (1–2), 49–62. http://dx.doi.org/10.1016/j.jvolgeores.2008.12.009.

Puglisi, G., Bonforte, A., Ferretti, A., Guglielmino, F., Palano, M., Prati, C., 2008. Dynamics of Mount Etna before, during, and after the July-August 2001 eruption inferred from GPS and differential synthetic aperture radar interferometry data. J. Geophys. Res.: Solid Earth 113 (6), 1–20. http://dx.doi.org/10.1029/2006JB004811.

Rançon, J.P., Lerebour, P., Augé, T., 1989. The Grand Brule exploration drilling: New data on the deep framework of the Piton de la Fournaise volcano. Part 1: Lithostratigraphic units and volcanostructural implications. J. Volcanol. Geotherm. Res. 36 (1–3), 113–127. http://dx.doi.org/10.1016/0377-0273(89)90008-5.

Richter, N., Froger, J.L., 2020. The role of interferometric synthetic aperture radar in detecting, mapping, monitoring, and modelling the volcanic activity of piton de la fournaise, la reunion: A review. Remote. Sens. 12 (6), http://dx.doi.org/10.3390/rs12061019.

Rivalta, E., Taisne, B., Bunger, A.P., Katz, R.F., 2015. A review of mechanical models of dike propagation: Schools of thought, results and future directions. Tectonophysics 638 (C), 1–42. http://dx.doi.org/10.1016/j.tecto.2014.10.003.

Roult, G., Peltier, A., Taisne, B., Staudacher, T., Ferrazzini, V., Di Muro, A., 2012. A new comprehensive classification of the Piton de la Fournaise activity spanning the 1985–2010 period. Search and analysis of short-term precursors from a broad-band seismological station. J. Volcanol. Geotherm. Res. 241–242, 78–104. http://dx.doi.org/10.1016/j.jvolgeores.2012.06.012.

Rousset, D., Lesquer, A., Bonneville, A., Lénat, J.F., 1989. Complete gravity study of Piton de la Fournaise volcano, reunion island. J. Volcanol. Geotherm. Res. 36, 37–52.

Rubin, A.M., Pollard, D.D., 1988. Dike-induced faulting in rift zones of Iceland and Afar. Geology 16 (5), 413–417. http://dx.doi.org/10.1130/0091-7613(1988)016<0413:DIFIRZ>2.3.CO;2.

Ruch, J., Wang, T., Xu, W., Hensch, M., Jónsson, S., 2016. Oblique rift opening revealed by reoccurring magma injection in central Iceland. Nat. Commun. 7 (September), http://dx.doi.org/10.1038/ncomms12352.

Siebert, L., 1984. Large volcanic debris avalanches: characteristics of source areas, deposits, and associated eruptions. J. Volcanol. Geotherm. Res. 22, 163–197.

Smittarello, D., Cayol, V., Pinel, V., Froger, J.L., Peltier, A., Dumont, Q., 2019. Combining InSAR and GNSS to track magma transport at basaltic volcanoes. Remote. Sens. 11 (19), 1–26. http://dx.doi.org/10.3390/rs11192236.

Solaro, G., Acocella, V., Pepe, S., Ruch, J., Neri, M., Sansosti, E., 2010. Anatomy of an unstable volcano from InSAR: Multiple processes affecting flank instability at Mt. Etna, 1994–2008. J. Geophys. Res.: Solid Earth 115 (10), 1994–2008. http://dx.doi.org/10.1029/2009JB000820.

Stieltjes, L., Moutou, P., 1989. A statistical and probabilistic study of the historic activity of Piton de la Fournaise, Reunion Island, Indian ocean. J. Volcanol. Geotherm. Res. 36 (1–3), 67–86. http://dx.doi.org/10.1016/0377-0273(89)90006-1.

Tibaldi, A., Groppelli, G., 2002. Volcano-tectonic activity along structures of the unstable NE flank of Mt. Etna (Italy) and their possible origin. J. Volcanol. Geotherm. Res. 115 (3–4), 277–302. http://dx.doi.org/10.1016/S0377-0273(01)00305-5.

Torgersen, E., Arctander, K., Redfield, T.F., Svendby, A.K., Dichiarante, M., Arntsen, M.L., 2024. Are all lineaments the surface expression of faults and fractures ? – A novel analysis using tunnel face mapping data from Norwegian road tunnels. In: EGU General Assembly. http://dx.doi.org/10.5194/egusphere-egu24-16840.

Tridon, M., Cayol, V., Froger, J.L., Augier, A., Bachèlery, P., 2016. Inversion of coeval shear and normal stress of Piton de la Fournaise flank displacement. J. Geophys. Res.: Solid Earth 121 (11), 7846–7866. http://dx.doi.org/10.1002/2016JB013330.

Urlaub, M., Geersen, J., Petersen, F., Gross, F., Bonforte, A., Krastel, S., Kopp, H., 2022. The submarine boundaries of Mount Etna's unstable southeastern flank. Front. Earth Sci. 10 (March), 1–17. http://dx.doi.org/10.3389/feart.2022.810790.

Valentine, G.A., Krogh, K.E., 2006. Emplacement of shallow dikes and sills beneath a small basaltic volcanic center - the role of pre-existing structure (Paiute Ridge, southern Nevada, USA). Earth Planet. Sci. Lett. 246 (3–4), 217–230. http://dx.doi.org/10.1016/j.epsl.2006.04.031.

Villeneuve, N., Bachelery, P., 2006. Revue de la typologie des éruptions au Piton de la Fournaise, processus et risques volcaniques associés. CyberGeo 1–25. http://dx.doi.org/10.4000/cybergeo.2536.

Walter, T.R., Haghshenas Haghighi, M., Schneider, F.M., Coppola, D., Motagh, M., Saul, J., Babeyko, A., Dahm, T., Troll, V.R., Tilmann, F., Heimann, S., Valade, S., Triyono, R., Khomarudin, R., Kartadinata, N., Laiolo, M., Massimetti, F., Gaebler, P., 2019. Complex hazard cascade culminating in the Anak Krakatau sector collapse. Nat. Commun. 10 (1), http://dx.doi.org/10.1038/s41467-019-12284-5.